# Wave front control techniques for imaging space objects at large zenith angles

Michael C. Roggemann, Grant Soehnel,
Glen E. Archer, Timothy J. Schulz *

September 10, 2006

**Abstract**

The problem of mitigating atmospheric turbulence-induced distortions from imagery measured by astronomical and space surveillance telescopes operating at high zenith angles is addressed here. Most previous research in this problem has emphasized operation at relatively small zenith angles, where turbulence effects are less severe, and effects arising from relatively weak phase distortions dominate the measurements. As the zenith angle increases the propagation path through the atmosphere gets progressively longer, with the result that the wave front arriving at the telescope is corrupted by both phase and amplitude fluctuations. This poses a problem for conventional adaptive optics systems because the assumptions implicit to their design and construction are violated. Our goal is to examine and compare the performance of two approaches to deformable mirror control  a conventional recursive technique, and the slope discrepancy technique. We created a closed loop adaptive optics imaging simulation of an AEOS-like adaptive optics system imaging a star at zenith angles in the range 0 - 70 degrees using both deformable mirror control paradigms, and compare performance. Our results show that the slope discrepancy wave front reconstructor provides significantly better performance at all zenith angles, but this performance advantage is particularly strong at high zenith angles.

## 1 Introduction

The success of adaptive optical systems in significantly reducing atmospheric turbulence-induced effects in astronomical and space surveillance images under

*All authors are with Michigan Technological University, Department of Electrical and Computer Engineering, 1400 Townsend Drive, Houghton, MI.

conditions where turbulence-induced phase effects dominate [1, 2, 3] has lead to interest in extending adaptive optics imaging capabilities to new regimes, where turbulence effects are stronger. Of particular interest is developing techniques to expand the field of regard of adaptive optical systems to increase the range of zenith angles where high quality object estimates can be obtained. The underlying physical problem is as follows: as the zenith angle $\theta_z$ of the observations increases, the optical path through the turbulent atmosphere increases. As a result, as $\theta_z$ increases the correlation length of the field arriving from the object of interest generally decreases, and the strength of turbulence-induced amplitude fluctuations, referred to as scintillation, generally increases. These effects impact the quality of the wave front measurement and should affect the choice of a deformable mirror control strategy.

In this paper we begin examing the performance tradeoff between two deformable mirror control algorithms - a conventional recursive algorithm which at high signal-to-noise ratio provides performance similar to the least squares reconstructor, and an algorithm which is sensitive to discontinuities in the phase map referred to as the slope discrepancy reconstructor [4]. To conduct this study we simulated a closed loop adaptive optics system similar to the AEOS telescope adaptive optics sytem. Wave optics models of the propagation and all optical elements was used to capture the effects of extended volume turbulence, and the resulting reduction in the field correlation length, and scintillation on system performance. The telescope was simulated as imaging an on-axis natural star, operating through turbulence modeled by the MAUI3 turbulence profile, and two times the MAUI3 turbulence profile, in the zenith angle range $0 \leq \theta_z \leq 70$ degrees.

As the zenith angle gets large in these trials, an important point is reached when the Fried parameter becomes smaller than the wave front sensor subaperture size projected to the pupil of the telescope. When this situation arises, the image formed by the wave front sensor lenslets generally becomes speckled, and the errors associated with the measurement of the local phase differences of the incoming field can become significant. Using least squares and recursive reconstructors in this situation generally results in severely reduced performance. We have found that using the slope discrepancy method results in significantly better performance in this regime, and anticipate that combining this approach with post detection image processing will further improve the quality of the object estimate.

The remainder of this paper is organized as follows. The next section provides the theoretical background for this paper. Details on the simulations performed will be given in Section 3. Results are presented in Section 4, and conclusions are drawn in Section 5.

## 2 Theoretical Background

As light travels through the turbulent atmosphere phase distortions in the wave front arise due to random variations in the index of refraction of the air [3].

This effect is presented at the aperture of the telescope as a dynamic wave front aberration which can strongly degrade the image quality obtained in the absence of adaptive optics compensation. When the combination of path length and turbulence strength is relatively weak, or concentrated near the aperture, phase effects dominate the wave front error. However, as the optical path through the turbulence increases amplitude fluctuations and discontinuities in the phase aberration falling on the aperture become inportant [5, 6]. There are three parameters that are generally used to characterize the optical properties of light that has traveled through turbulence. These parameters are the Fried parameter $r_0$, the isoplanatic angle $\theta_0$, and the variance of the log-amplitude fluctuations in the aperture $\sigma_\chi^2$, also referred to as the Rytov variance [7]. Under conditions where phase effects dominate the turbulence-induced wave front error the Fried parameter $r_0$ is the maximum aperture diameter for which nearly diffraction limited images can be measured through the turbulence. The expression for $r_0$ is

$$r_0 = 2.1 \left[ 1.46 \sec(\phi) k^2 \int_0^L C_n^2(z)\, dz \right]^{-3/5}, \tag{1}$$

where $C_n^2(z)$ is the structure constant of the turbulence and a function of altitude, $z$. The isoplanatic angle $\theta_0$ is a measure of the largest angle separating two optical paths that can be assumed to experience approximately the same turbulence distortions, and is given by

$$\theta_0 = \left[ 2.914 k^2 \sec(\phi)^{8/3} \int_0^L C_n^2(z) z^{5/3}\, dz \right]^{-3/5}. \tag{2}$$

The Rytov variance $\sigma_\chi^2$ is a measure of the strength of the scintillation, and is given by

$$\sigma_\chi^2 = 0.563 k^{7/6} \left[ \sec(\phi) \right]^{11/6} \int_0^L C_n^2(z) z^{5/6}\, dz. \tag{3}$$

In the range $0 \leq \sigma_\chi^2 \leq 0.1$ the amplitude fluctuations are generally considered negligible. In the range $0.1 \leq \sigma_\chi^2 \leq 0.3$ scintillation can not be neglected, and in this regime advanced wave front reconstruction paradigms applied to the deformable mirror control problem can yield improved performance compared to least squares reconstruction [8, 9]. While the expression in Eq. 3 indicates that $\sigma_\chi^2$ increases with increasing turbulence strength and path length, experimental observations have shown that fluctuations in the log-amplitude of the field at a point saturate in the vicinity of $\sigma_\chi^2 \approx 0.3$ [7]. In this regime, amplitude effects can not be neglected, and discontinuities in the wave front arriving at the aperture are expected [5].

In this paper the optical path is represented by propagation from a star, through the MAUI3 turbulence profile, and through a turbulence profile given by two times the MAUI3 profile, to a telescope simulating the AEOS system at an altitude of 3 km above sea level. MAUI3 is a model for structure constant of the turbulence, $C_n^2(z)$, where $z$ is the altitude, above the AEOS observatory

at Mt. Haleakala. The MAUI3 turbulence profile is shown in Fig. 1. The atmospheric optics parameters $r_0$, $\theta_0$, and $\sigma_\chi^2$ are calculated for the MAUI3 profile at the mean AEOS wave front sensor wavelength of 650 nm, and two times the MAUI3 profile, and are presented in Fig. 2. Inspection of Fig. 2 shows that conditions where $r_0$ is less than the AEOS wave front sensor subaperture side length projected into the pupil of 11.4 cm can arise at virtually all $\theta_z$ for turbulence characterized by two times the MAUI3 turbulence profile, and for $\theta_z > 60$ deg for for turbulence characterized by the MAUI3 turbulence profile. Additionally, scintillation is non-negligible for $\theta_z > 60$ deg.

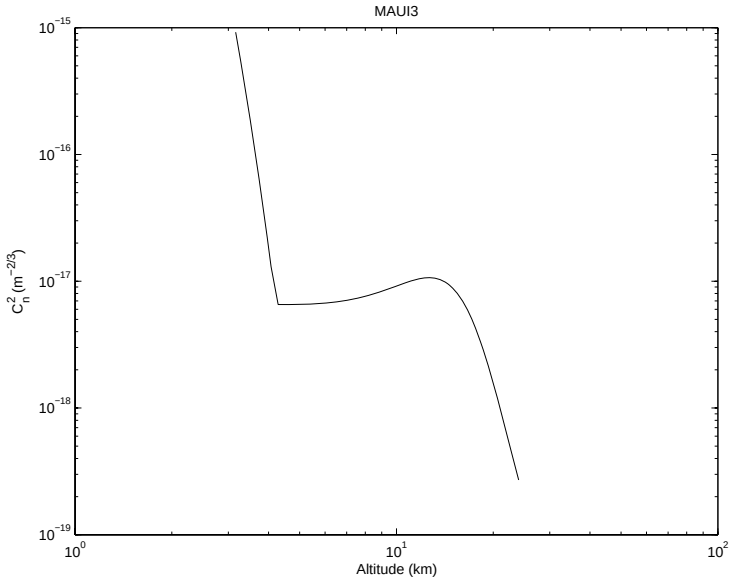


Figure 1: MAUI3 $C_n^2(z)$ profile.

To expand the range of useful $\theta_z$ for AEOS, and likely other telescopes, consideration must be given to the fact that the subaperture size and wave front reconstruction paradigms were selected with weak turbulence conditions in mind. When $r_0$ is smaller than the subaperture size, or when scintillation is strong, the assumptions of the widely used least squares reconstruction paradigm that the phase difference measurements are linear with respect to the local tilt, and that the turbulence induced phase error can be reasonably modeled as a continuous function are violated. Here, we seek to examine the role of the so-called slope discrepancy reconstructor [4] in a closed loop adaptive optics system for improving performance compared to a recursive reconstructor, which a reasonable approximation of a least squares reconstructor [3] at high signal-to-noise ratios. Both reconstructors process an array of phase difference measurements which, in the present case, are obtained from a simulated Hartmann wave front sensor. The recursive reconstructor starts in the middle of the

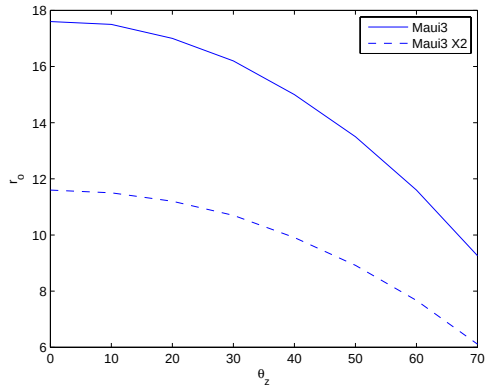


(a)

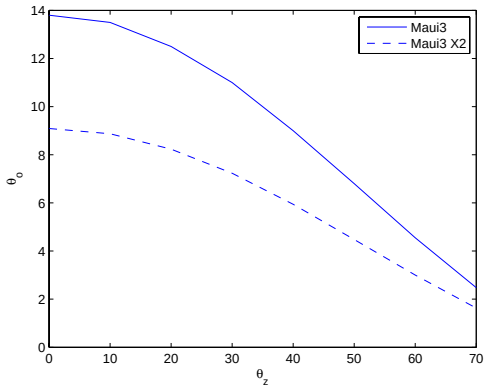


(b)

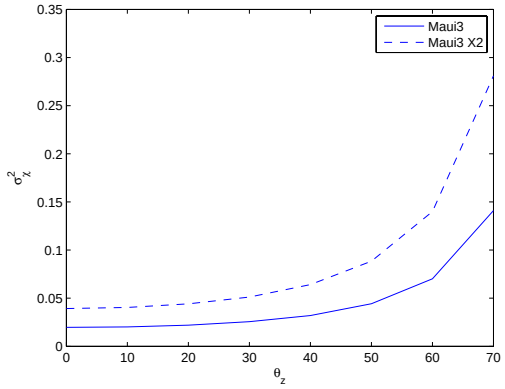


(c)

Figure 2: Atmospheric optics parameters as a function of zenith angle for the MAUI3 turbulence profile, and two times MAUI3: (a) $r_0$; (b) $\theta_0$. ; and (c) $\sigma_\chi^2$.

array of phase differences, and assigns the phase at this point to be zero. Phase differences are then summed in all directions away from the center to create a complete phase estimate. The slope discrepancy reconstructor employs both the recursive recontructor and the so-called exponential reconstructor described in reference [10]. The slope discrepancy method splits the phase estimate into the sum of two parts: (1) a phase due to the least squares estimate obtained from the phase differences measured by the wave front sensor, and (2) the slope discrepancy part. The least squares component of the phase is found by applying the recursive reconstructor to the array of phase differences obtained from the wave front sensor. Under conditions of significant scintillation it has been found that the least squares estimate of the phase can be improved by adding a component arising from the difference between the measured phase differences $\Delta\vec{\phi}$, and the phase differences which would be obtained if the least squares estimate of the phase were actually falling on the wave front sensor $\Delta\vec{\phi}_{LS}$. Computing the phase differences associated with the least squares estimate requires an accurate model of the wave front sensor, which is available in our simulation environment. When $\Delta\vec{\phi} - \Delta\vec{\phi}_{LS} \neq 0$ this difference is called the the slope (or, equivalently, the phase difference) discrepancy $\Delta\vec{\phi}_{SD}$. In the slope discrepancy reconstructor, $\Delta\vec{\phi}_{SD}$ is used as input to the exponential reconstructor which, in turn gives the slope discrepancy phase, which is added to the least squares phase estimate to obtain the total reconstructed phase. We note that the slope discrepancy reconstructor contains considerable complexity not discussed here. We refer the readers to the literature, particularly the excellent references [4] and [10]. This reconstructed phase is used to create a set of commands for the deformable mirror, which is used to correct the phase of the incoming field before an image is formed. The wave front sensor, deformable mirror, control loop, and image formation models used here have been widely used, and are described in detail in other papers [3, 9, 11, 12, 13]. We provide the details of the various parameters used in these models in the next section, where the simulation is described.

# 3 Simulation Approach

In this section we describe the simulation. The three dimensional volume of the atmosphere is modeled here by 10 equally spaced phase screens whose strength is characterized by value of $r_0$ for each layer. The lowest layer lies in the telescope pupil, and the layers above are equally spaced. The value of $r_0$ for each layer is calculated using Eq. 1. The temporal dynamics of the atmosphere are modeled using Taylors frozen flow hypothesis [3]. The transverse air motion is modeled here as uniform across the vertically stacked layers, allowing the phase screens shifted uniformly to obtain the turbulence characteristics as a function of time. Random phase screens were generated to have the Kolmogorov power spectral density using a widely available technique [15, 16]. The adaptive optics model is run in a closed loop mode such that the wave front sensor measures light after it has been corrected by the current figure of the deformable mirror.

To study the effects of increasing scintillation on the phase reconstruction techniques and the image reconstruction, the propagations were run at various values of $\theta_Z$, from $0 \leq \theta_Z \leq 70$ degrees in 10 degree increments. In this case it was assumed that the sampling rate of the wave front sensor is 1 kHz, and each time shift of 1 ms corresponds to a one pixel shift. The sample spacing in the atmospheric model was set at 8 mm, and hence, this choice results in an 8 m/s wind velocity. A circular shift was implemented so that the column of phase data lost off the right edge is wrapped around to the left edge each time.

The program begins and initializes with the following steps.

1. The optical and geometry parameters are defined. The turbulence lies in the altitude range from 3000 m to 20000 m. The wave front sensor wavelength is 650 nm and the imaging wavelength is 850 nm. The diameter of the primary aperture was set at 3 m.

2. The angular spectrum transfer function for the propagator is created.

3. The incident field is created, which in this case consists of a set of plane waves falling on the top of the atmosphere from different directions to simulate a field of randomly placed stars.

4. The adaptive optics configuration is initialized. The wave front sensor lenslet transfer function is created. The subapertures are 15 samples across, or 12 cm on a side when projected into the pupil plane. There are 27 subapertures across the diameter of the telescope pupil. Deformable mirror actuator influence functions are modeled as linear splines with base width equal to the subaperture side length, and they are placed at the corners of the subapertures. This results in 445 subapertures and 484 actuators present inside the filled pupil. A wave optics model for the wave front sensor is also used, requiring the creation of the complex transmittance of the lenslet array, and an angular spectrum propagator to move the field from the back of the lenslet array to the detector plane of the wave front sensor.

5. A plane wave is propagated through the wave front sensor to obtain a calibration to be used later.

6. A vector of turbulence weights is calculated along with $r_o$ for each of the 10 turbulence layers.

7. A circular pupil of 3 m diameter is created to represent the actual telescope aperture.

At this point the program enters a the main loop, which iterates over independent realizations of the atmosphere volume. Next the program enters an inner loop which models the dynamics of the atmosphere and the adaptive optics system.

1. The phase screens are circularly shifted to represent a time step in the turbulence.

2. A plane wave representing a on-axis beacon for the wave front sensor is propagated through the simulated turbulence to the telescope aperture. The incident field due to the stars is also propagated to the telescope aperture.

3. A square centered subwindow is cut out of both the wave front sensor field and the star field. It is the same size as the square lenslet transfer function. The sizes were chosen to make sure that the entire subwindow is inside the propagation roll off function.

4. The overall tilt of the wavefront is estimated from the beacon light using an centroid tracker, and the resulting tilt correction is applied to the incoming field due to the stars. The tiltcorrected field falls on deformable mirror model, and then the wave front sensor model, and phase difference measurements are computed.

5. The phase differences are sent to a recursive reconstructor to calculate an approximation to the least squares phase reconstruction, and this estimate along with the measured phase differences are used to calculate the slope discrepancy reconstructor estimate of the phase. It should be noted that both reconstructors are designed to provide phase estimates on a low resolution grid, at the corners of the subapertures.

6. The deformable mirror is exists at the resolution of the simulation. The figure of the deformable mirror computed for each reconstructor by assigning the estimated phase at the corner of the subaperture as the weight for each actuator.

7. When the number of time steps in the inner loop has reached 25 it is assumed that the system has stabalized and the first intensity images are formed. Four images are formed: an on-axis point spread function due to the beacon light for each reconstructor, and an image of the compensated star field for each reconstructor. Subsequent shifts of the atmosphere and corrections by the adaptive optics result in new realizations of the image which are accumlated to obtain the average noise free image of the star field.

The above steps of the inner loop run 150 times, representing 150 time shifts. Once this is completed the outer loop creates a new, independent set of 10 phase screens and then the inner loop runs again with the new phase screens. This has been done in order to average over independent realizations of the atmospheric turbulence.

# 4 Results

We now present the results of our studies to date. Figure 3 shows the set of time averaged PSFs as a function of $\theta_Z$ for the MAUI3 turbulence profile for:

(a) the recursive reconstructor; and (b) the exponential reconstructor. Figure 4 shows a similar set of results for imaging through turbulence characterized by two times the MAUI3 turbulence profile. Comparison of Figs. 3(a) and (b), and Figs. 4(a) and (b) shows the interesting result that the slope discrepancy reconstructor is always better than the recursive reconstructor, and in cases where the scintillation is not negligible, the slope discrepancy reconstructor is much better. For example, at $\theta_Z = 70$ deg, the on-axis PSF for the slope discrepancy reconstructor is approximately a factor of 10 bigger than the on-axis PSF for the recursive reconstructor case. This observation provides motivation for finding fast implementations of the slope discrepancy reconstructor on widely used array processor-type computers used in adaptive optics real time wave front reconstruction and deformable mirror control systems.

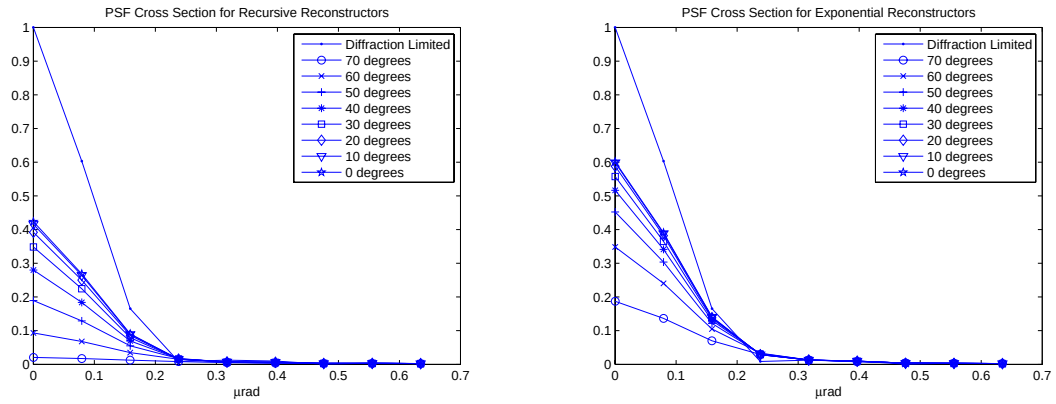


(a) (b)

Figure 3: (a) Average PSFs for the recursive reconstructor as a function of $\theta_Z$ for the MAUI3 turbulence profile; and (b) average PSFs for the slope discrepancy reconstructor as a function of $\theta_Z$.

# 5 Conclusion

We have examined the comparative closed loop performance of the recursive and slope discrepancy reconstructors as a function of zenith angle for an AEOS-like system imaging through the MAUI3 turbulence profile. Our studies have shown that the slope discrepancy reconstructor is superior to the recursive reconstructor at all zenith angles, and it is much better for $\theta \geq 50$ deg. This observation may motivate studies of how to implement the slope discrepancy reconstructor in real adaptive optics hardware.

# References


[1] Robert K. Tyson. *Principles of Adaptive Optics, Second Edition.* Academic Press, Inc., Boston, MA, 1998.

[2] V. P. Lukin. *Atmospheric Adaptive Optics.* SPIE Press, Bellingham, WA, 1995.

[3] M. C. Roggemann and B. M Welsh. *Imaging Through Turbulence.* CRC Press, Boca Raton, FL, 1996.

[4] G. A. Tyler. Reconstruction and assessment of the least-squares and slope discrepancy components of the phase. *J. Opt. Soc. Am. A*, 17:1828–1839, 2000.

[5] D. L. Fried. Branch point problem in adaptive optics. *J. Opt. Soc. Am. A*, 15:2759–2768, 1998.

[6] D. L. Fried and J. L. Vaughn. Branch cuts in the phase function. *Appl. Opt.*, 31:2865–2882, 1992.

[7] R. R. Beland. Propagation through atmospheric optical turbulence. In F. G. Smith, editor, *IR/EO Handbook*, volume 2, pages 157–232. SPIE Press, Bellingham, WA, 1993.

[8] M. C. Roggemann and A. C. Koivunen. Branch point reconstruction in laser beam projection through turbulence with finite degree of freedom phase only wave front correction. *J. Opt. Soc. Am. A*, 17:53–62, 2000.

[9] M. C. Roggemann and A. C. Koivunen. Wave front sensing and deformable mirror control in strong scintillation. *J. Opt. Soc. Am. A*, 17:911–919, 2000.

[10] D. L. Fried. Adaptive optics wave function reconstruction and phase unwrapping when branch points are present. *Opt. Commun.*, 200:43–72, 2001.

[11] R. T. Brigantic, M. C. Roggemann, K. W. Bauer, and B. M. Welsh. Image quality metrics for characterizing adaptive optics system performance. *Appl. Opt.*, 36:6583–6593, 1997.

[12] R. T. Brigantic, M. C. Roggemann, K. W. Bauer, and B. M. Welsh. Optimization of adaptive optics systems closed loop bandwidth to maximize imaging system performance. *Appl. Opt.*, 37:848–855, 1998.

[13] M. C. Roggemann and T. J. Schulz. Algorithm to increase the largest aberration which can be reconstructed from hartmann sensor measurements. *Appl. Opt.*, 37:4321–4329, 1998.

[14] T. J. Schulz. Multiframe blind deconvolution of astronomical images. *J. Opt. Soc. Am. A*, 10:1064–1073, 1993.

[15] Gregory Cochran. Phase screen generation. Technical Report TR-663, The Optical Sciences Company, Placentia, California, 1985.

[16] T. J. Brennan and P. H. Roberts. *AOTOOLs: The Adaptive Optics Toolbox*. the Optical Sciences Company, 1341 South Sunkist St., Anaheim, CA 92806, 1999.

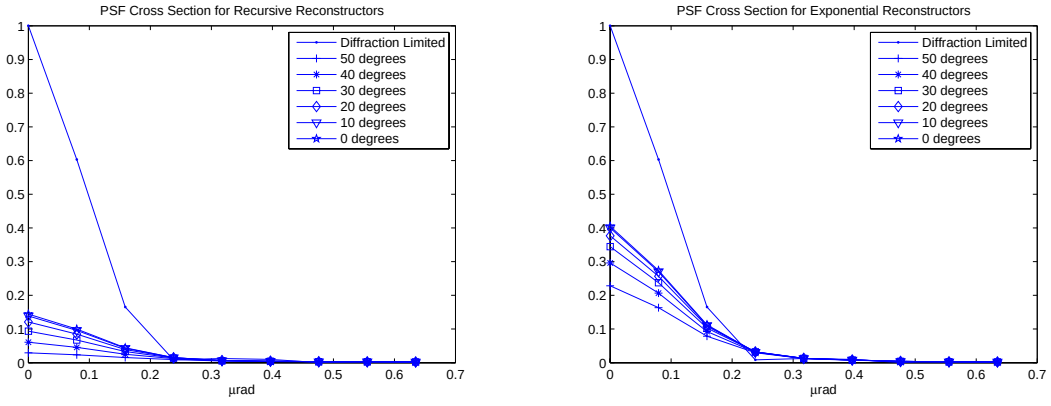


(a) (b)

Figure 4: (a) Average PSFs for the recursive reconstructor as a function of $\theta_Z$ for two times the MAUI3 turbulence profile; and (b) average PSFs for the slope discrepancy reconstructor as a function of $\theta_Z$.